Single transverse mode control of VCSEL by photonic crystal and trench patterning

Mohd Sharizal Alias [a,*], Sahbudin Shaari [b], Paul O. Leisher [c], Kent D. Choquette [d]

[a] *Microelectronics & Nanotechnology Program, Telekom Malaysia Research & Development (TMR&D), Lingkaran Teknokrat Timur, 63000 Cyberjaya, Selangor, Malaysia*
[b] *Institute of Microengineering & Nanoelectronics (IMEN), National University of Malaysia (UKM), 43600 Bangi, Selangor, Malaysia*
[c] *nLight Corporation, 5408 NE 88th St., Bldg. E, Vancouver, WA 98665, USA*
[d] *Electrical & Computer Engineering Department, University of Illinois at Urbana Champaign (UIUC), Urbana 61801, IL, USA*

Abstract

Single transverse mode control is achieved for multimode GaAs-based VCSEL by utilizing photonic crystal design and etched trench structure. Theoretical analysis is initially performed for photonic crystal design with various lattice constants and air holes diameter. The fabricated photonic crystal VCSEL with etched trench structure exhibits single mode output power of 0.7 mW, threshold current of 3.5 mA, slope efficiency of 0.10 W/A, and continuous single mode output spectrum throughout a wide operating current range. Comparison of typical oxide VCSEL, trench oxide VCSEL, and photonic crystal oxide VCSEL employing trench structure is presented. By combining photonic crystal and trench structure, single transverse mode operation of photonic crystal VCSEL can be much more strictly controlled.
© 2010 Elsevier B.V. All rights reserved.

Keywords: VCSEL; Photonic crystal; Semiconductor laser; GaAs

1. Introduction

Since the invention of Vertical-Cavity Surface-Emitting (VCSEL) in late 1970s [1], it has dominated the light source market for data communication such as Gigabit Ethernet and Fiber Channel. VCSEL are becoming attractive low cost and high performance light source for long wavelength optical communication, optical interconnect, automotive network, optical mouse, gas spectroscopy, and high definition display [2–4]. These promising developments are due to VCSEL advantages of low operating current and power consumption, high fiber coupling efficiency, high modulation bandwidth, 2D arrays capability, and low cost yet high-yield manufacturing ability (on wafer test and similar microelectronics device processing).

Single transverse mode operation of VCSEL is significant for efficient coupling into the central low modal dispersion region of multimode fiber [5] or for coupling into single mode fiber which has a smaller core diameter. Typical commercial multimode VCSEL nowadays used 10–20 μm oxide aperture technique for index- and current-confinement scheme [6,7]. To achieve single transverse mode operation, the oxide aperture of VCSEL must be less than 4 μm [8]. This stringent condition leads to low power output due to small aperture, high optical losses due to scattering, and introduce high resistance which reduces the high speed capability. Recently, various methods are reported for achieving single transverse mode VCSEL by introdu-

---

* Corresponding author.
E-mail address: sharizal@tmrnd.com.my (M.S. Alias).

cing losses to the higher order modes such as proton implanted structure [9], surface-relief etching [10,11], hybrid oxide-implant VCSEL [12], holey structure [13,14], and photonic crystal air holes [15–18].

In this paper, we report on single transverse mode photonic crystal VCSEL (PhC VCSEL) utilizing trench patterning and fan-pad metallization. VCSEL with trench structure exhibits higher device efficiency and highly confined multimode spectra in comparison to square air post mesa in typical oxide VCSEL [19]. This is due to narrower mode confinement provided for such structure compared with a given square air post mesa VCSEL. Furthermore, the usage of fan-pad metallization can increase high speed operation by reducing current resistance. By combining these advantages of device geometry (trench structure) with photonic crystal (PhC) air holes etched onto the VCSEL top Distributed Bragg Reflector (DBR) mirror, significant control of single transverse mode PhC VCSEL is realized. To the best of our knowledge, this is the first comprehensive reported work on theoretical analysis and experimental development of this kind of PhC VCSEL (with etched trench). Most of previous reported PhC VCSEL is based on air post mesa structure.

2. Photonic crystal design and device fabrication

2.1. Photonic crystal design

Single mode operation in PhC VCSEL can be realized similar to PhC optical fiber concept [20] by creating 2D arrays of air holes onto the top DBR mirror. The PhC structure creates a step refractive index profile across the VCSEL device. In addition, it introduces optical losses to high order modes, allowing only single fundamental mode condition [17]. Detail design of the studied PhC design is shown in Fig. 1, with design parameters consideration of triangular lattice constant, a, and air hole diameter, b. The transverse index around a single defect point can be controlled by the air hole diameter to lattice constant ratio (b/a). We fixed the b/a ratio at 0.5 by varying a and b dimensions; and assuming the VCSEL circular diameter is 43 μm, oxide aperture is 9 μm, average top DBR refractive index of 3.2775, and oxide layer refractive index of 1.75. The theoretical analysis is performed using Plane Wave Expansion (PWE) method [21] and Finite Difference Frequency Domain (FDFD) method [22].

2.2. VCSEL device fabrication

The 850 nm oxide VCSEL epiwafer consists of three GaAs quantum wells and four $Al_{0.3}Ga_{0.7}As$ barriers forming the active region which is sandwiched between 34.5 periods of bottom n-type and 25 periods of top p-type DBR mirrors. The DBR mirrors composed of alternating high- and low-refractive index layers of $Al_{0.15}Ga_{0.85}As/Al_{0.9}Ga_{0.1}As$ multilayer. A high aluminum concentration layer of $Al_{0.98}Ga_{0.02}As$ is introduced in the p-DBR mirror adjacent to the active region for selective oxidation purpose. Three types of oxide VCSEL devices are fabricated which is typical air post mesa VCSEL (sample T1), VCSEL with trench patterning (sample T2), and PhC VCSEL with trench patterning (sample T3). The cross-section for respective device is schematically illustrated in Fig. 2.

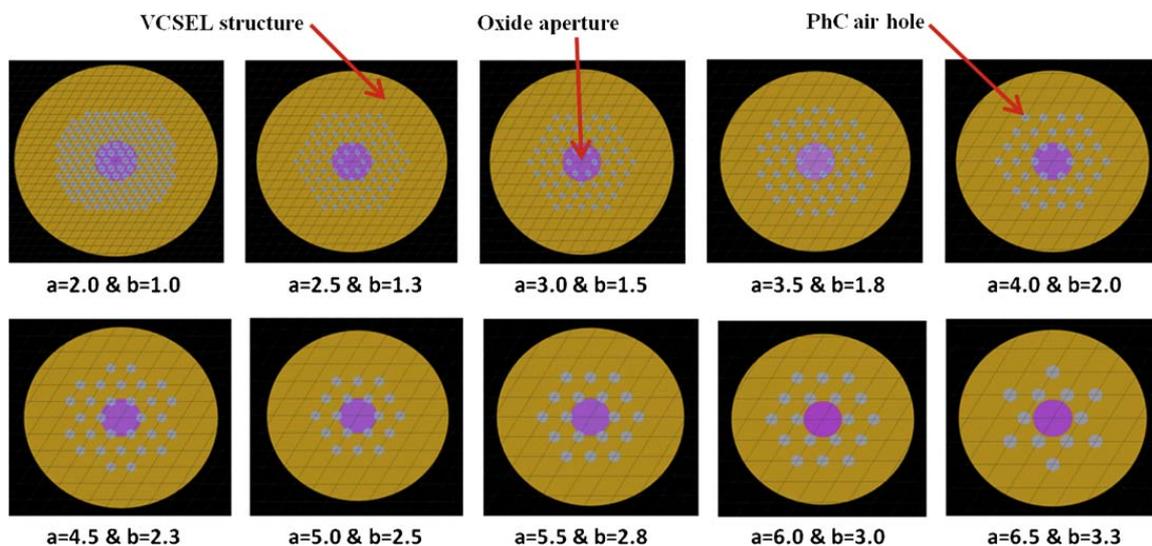Fabrication processes for all three 850 nm oxide VCSEL devices (samples T1–T3) are similar with the

Fig. 1. PhC design for various b/a ratios of 0.5 μm and 9 μm oxide aperture.
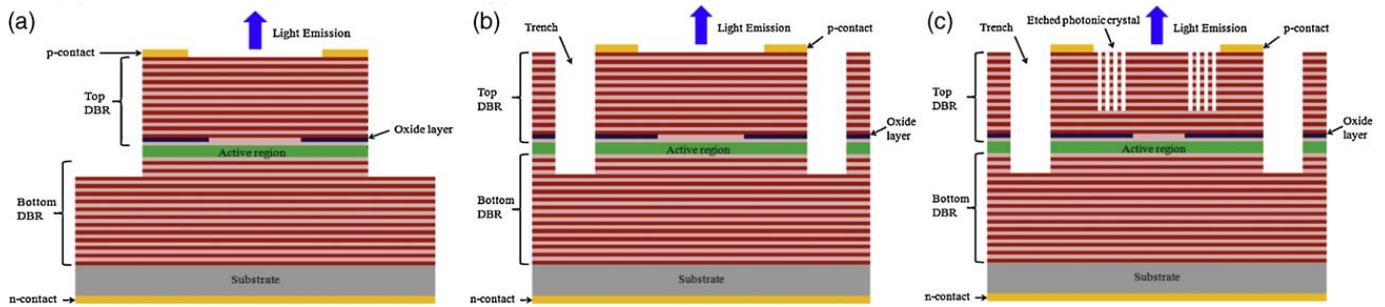
Fig. 2. The oxide VCSEL devices with (a) air post mesa, (b) trench structure, and (c) PhC and trench structure.

only difference in the photomask design used and additional photolithography steps required for VCSEL samples T2 and T3. Detail fabrication is only described for PhC VCSEL with trench patterning since fabrication steps for VCSEL samples of T1 and T2 have been reported previously [19]. The device fabrication started with the metallization of the bottom n- and the top ring p-ohmic contacts by evaporating AuGe/Ni/Au (40/20/150 nm) and Ti/Au (15/150 nm), respectively. The bottom n-contact is straightforward deposition; however the top p-contact required photolithography patterning and lift-off process. In order to isolate adjacent devices, the surface of the VCSEL epiwafer is proton implanted. First, SiO_2 mask is deposited by the process of plasma-enhanced chemical vapor deposition (PECVD). Then, all VCSEL apertures are protected by thick photoresist pillars (formed on the top ring contact) prior to implantation. After proton implantation, the photoresist pillars are removed and thick SiO_2 mask is re-deposited by PECVD. PhC holes and trench patterning are then transferred (single step photolithography) to SiO_2 mask followed by reactive ion etching (RIE) mask etched. The leftover photoresist is removed and thicker photoresist pillars are formed on the top ring contacts to protect the PhC holes mask patterns prior to trench etching by inductively coupled plasma RIE (ICP-RIE). After trench is partly etched, the thick photoresist

pillars are removed. The epiwafer is then exposed to wet oxidation process for forming the oxide aperture. Next, PhC air holes are etched onto the VCSEL aperture by second ICP-RIE process (trench will completely etched at the same time) followed by SiO_2 mask removal by RIE. The PhC VCSEL with trench patterning device fabrication is completed by defining the fan-pad metallization (formed by photolithography, evaporation of Ti/Au of 25/1000 nm and metal lift-off).

Fig. 3 shows the scanning electron microscope (SEM) images for all three types of 850 nm oxide VCSEL fabricated devices (samples T1–T3). Each sample is tilted at different angles to effectively demonstrate the air post square mesa structure, the circular mesa and etched trench, and PhC air holes for the respective devices. Fig. 4 displays optical microscope images (top view) for all incorporated PhC designs for *b/a* ratio of 0.5 fabricated along the PhC VCSEL with trench patterning (prior to fan-pad metallization). The PhC air holes are fabricated exactly as in the computed PhC designs for *b/a* ratio of 0.5 (refer to Fig. 1). This will ensure that the fabricated PhC VCSEL operates in single mode as expected from the theoretical study.

The VCSEL device measurement is performed on wafer probing system at room temperature under continuous wave operation. The light versus current
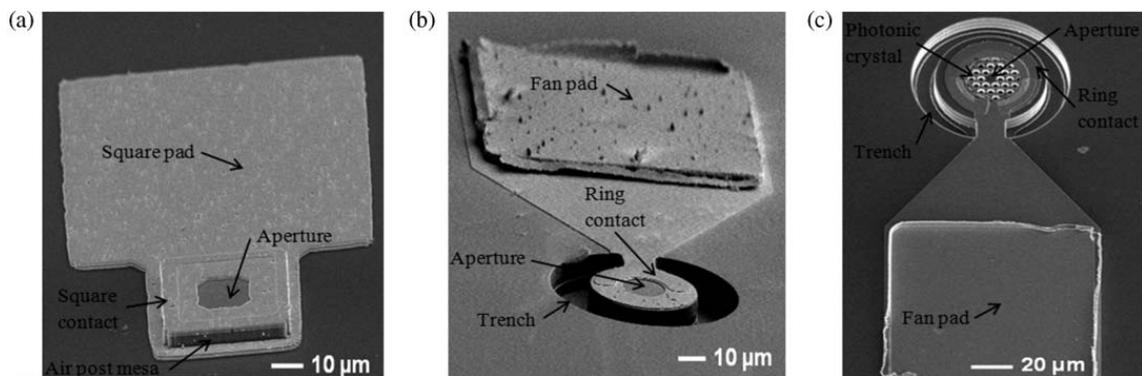

Fig. 3. SEM images for the fabricated (a) air post mesa VCSEL, (b) trench VCSEL, and (c) PhC VCSEL with trench.
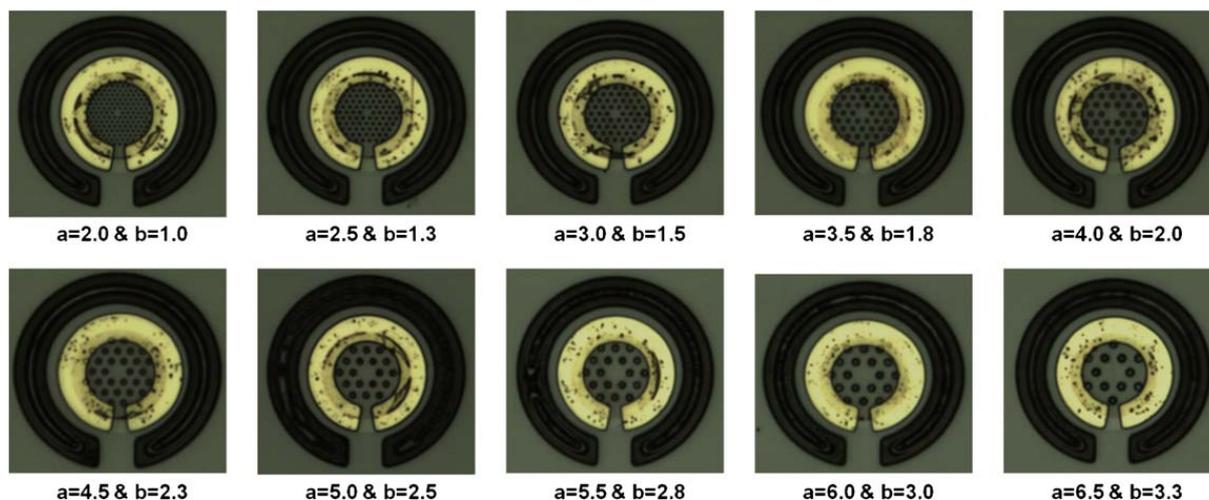
Fig. 4. Top view optical images for all fabricated PhC designs of *b/a* = 0.5 for the PhC VCSEL.

(*L–I*) and current versus voltage (*I–V*) characteristics are measured with the precise variation of input current (using semiconductor parameter analyzer). The light output is detected by silicon photodetector which is also connected to the semiconductor parameter analyzer. The output spectrum of VCSEL is obtained by coupling the lasing beam into an optical fiber connected to an optical spectrum analyzer.

3. Results and discussion

3.1. Photonic crystal design

Fig. 5 shows the out of plane photonic band diagram (PBG) computed using PWE method for all PhC triangular periodic lattice designs of *b/a* ratio = 0.5 with single point defect and the assumption of infinite holes etched. This is a simplified approximation to describe the optical behavior of the VCSEL top DBR mirror that

has been etched with PhC air holes. The area under each linear curve (lower right half) is defined by a line which refers to the lowest order out of plane mode for each PhC air holes design. The slope of this line represents an effective index of the structure formed by the PhC air holes which induced index guiding effect. Higher effective index is obtained as the lattice constant and holes diameter increased. By purposely introduced point defect at centre of the index guiding region (unetched air hole); higher index waveguide confinement is realized. Fig. 6 exhibits the fundamental mode profiles for each of the PhC design for *b/a* ratio of 0.5 computed using FDFD method. Defect modes can appear inside the index guiding region with proper PhC air holes design.

In case of PhC VCSEL, the effective index computed from the PBG diagram corresponds to the refractive index (assumed as n_{clad}) for area of the top DBR region etched with PhC structure. The refractive index
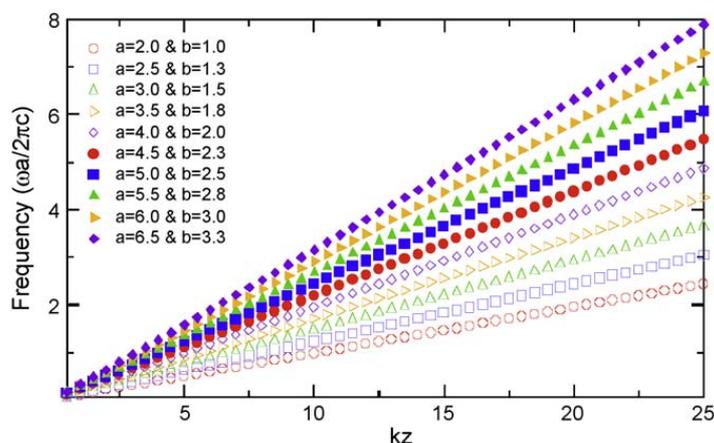

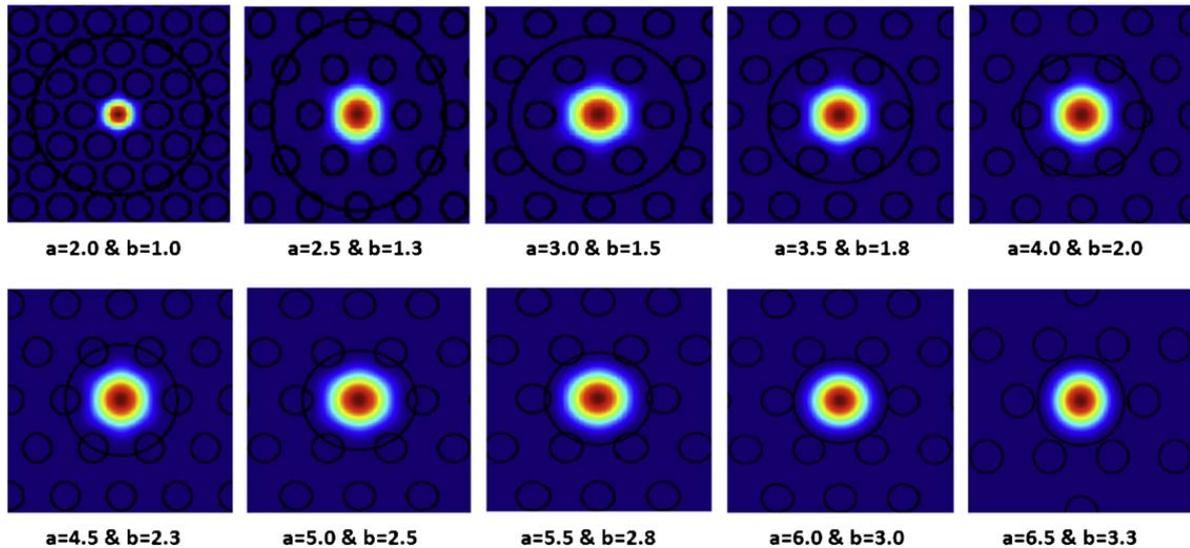Fig. 5. PBG diagram of PhC structure with out of plane propagation for all PhC designs of *b/a* = 0.5.

Fig. 6. Fundamental transverse mode profile for all PhC designs of $b/a = 0.5$.

(assumed as n_{core}) for the unetched region (no point defect) is obtained by averaging the high- and low-refractive index multilayer used for the DBR materials. This approach is similar to step index cylindrical waveguide in optical fiber. Due to this similarity, the normalized frequency or V_{eff} parameter [23] as defined in Eq. (1) can be used to determine the number of confined modes (single mode expected if $V < 2.405$), where D is the defect diameter ($2a - b$), λ is the operating wavelength, n_{clad} and n_{core} as described above.

$$V_{eff} = \frac{\pi D}{\lambda} \sqrt{n_{core}^2 - n_{clad}^2} \qquad (1)$$

However in PhC fiber, the air holes are etched thoroughly (infinite). In PhC VCSEL, the top DBR mirror is only 50–80% etched with air holes due to the fabrication limitations and to avoid high optical losses inside the VCSEL. Due to this consideration (finite etch depth), Eq. (1) is modified by introducing etch depth factor, γ, as calculated in Eq. (2) [24].

$$V_{eff} = \frac{\pi D}{\lambda} \sqrt{n_{core}^2 - [(1 - \gamma)n_{core} + \gamma n_{clad}]^2} \qquad (2)$$

In order to compute the V_{eff} parameter for all PhC designs of b/a ratio = 0.5, D is calculated from the given a and b dimension in Fig. 1, λ is at 850 nm, n_{core} is 3.2775, n_{clad} is calculated from PBG diagram for every PhC design, and γ is assumed as 0.1 (19 DBR pairs etched) [24]. In order to simplify the calculation, the effect of trench structure and optical loss is not taken into account. The trench structure is considered to minimize the number of supported high order modes but

not a significant factor in realizing single mode operation (as shown in the experimental result later). Thus the effect of trench structure is neglected and the geometry of the device is assumed like air post mesa in the calculation. The optical loss factor is recently taken into consideration for the V_{eff} parameter calculation [25]. The calculation is simplified in this paper since the purpose is only to provide general analysis of our PhC air holes design. Fig. 7 shows the calculated V_{eff} parameter for all PhC designs of b/a ratio = 0.5. All PhC designs exhibit single mode behavior ($V_{eff} < 2.405$). By incorporating these PhC designs into the multimode VCSEL, single fundamental mode operation can be achieved.

3.2. Photonic crystal VCSEL experiment

Fig. 8 shows the *L–I* characteristic for fabricated 850 nm oxide VCSEL devices of typical air post mesa (sample T1), VCSEL with trench (sample T2), and PhC VCSEL with trench (sample T3). All VCSEL samples have 9 μm diameter of oxide aperture. VCSEL sample T3 is composed of PhC design of b/a ratio = 0.5 with $a = 4.0$ μm and $b = 2.0$ μm. VCSEL of samples T1 and T2 exhibits threshold current (I_{th}) of 0.8 mA, slope efficiency of 0. 29 W/A, and maximum output power (P_{max}) of 3.5 mW and 3.0 mW, respectively. VCSEL sample T3 achieved I_{th} of 3.5 mA, slope efficiency of 0.10 W/A, and P_{max} of 0.7 mW. The high I_{th} and low slope efficiency in PhC VCSEL is because higher optical threshold gain is required to compensate high order mode loss [17]. In addition, the etched PhC holes increased scattering loss [26] which also results in
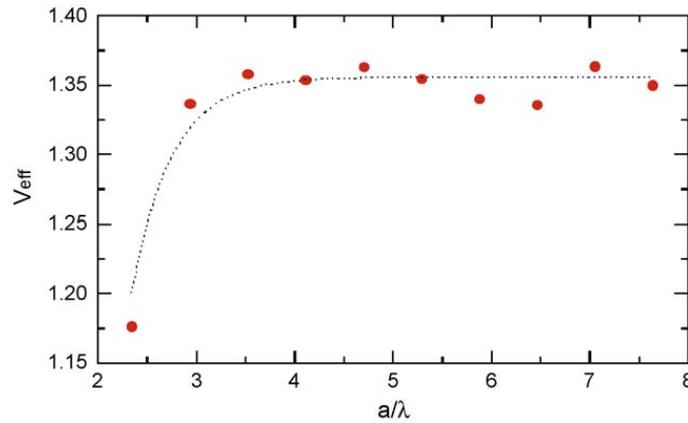
Fig. 7. V_{eff} parameter for all PhC designs of $b/a = 0.5$.

higher threshold current required to ensure lasing. P_{max} for sample T3 is low compared to others since only fundamental mode is allowed for lasing and modal volume decreased due to the existence of PhC air holes structure. However, the power composed of genuine single mode operation. The output power can be improved by optimizing device parameters such as oxide aperture, etch depth and PhC design.

The *I–V* characteristic as depicted in Fig. 9 shows slightly higher series resistance (slope of *I–V* curve) is

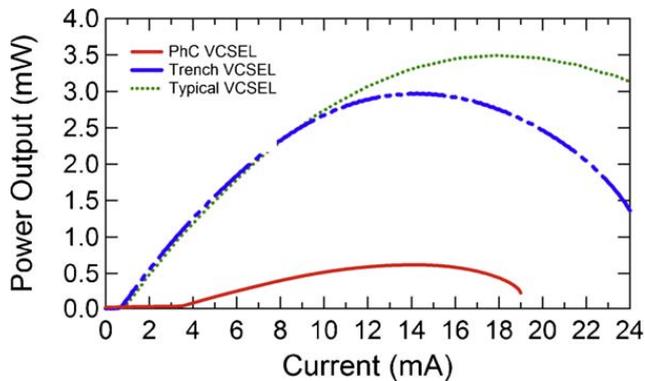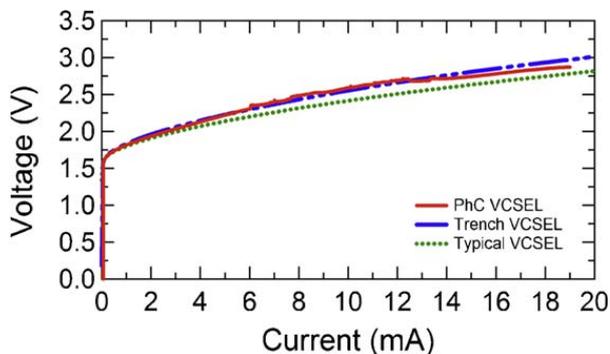obtained for both VCSEL samples T2 and T3 compared to sample T1. This is due to the introduction of resistance to the current flow by the PhC air holes and the etched trench structure. In addition, the etching of PhC air holes partially removed the conductive material of p-doped AlGaAs in the top DBR mirror.

Fig. 10 exhibits output spectrum for all fabricated VCSEL samples above threshold. Although both samples T1 and T2 are multimode VCSEL, better mode confinement is achieved by VCSEL with trench due to circular device geometry and stringent mode control (less high order modes supported). Almost 70% of the high order modes in the multimode VCSEL are eliminated. By combining the trench structure with etched PhC air holes in VCSEL, highly defined single mode condition is easily realized (as shown in the spectrum). Single mode condition is defined if more than 30 dB difference in side mode suppression ratio (SMSR) is achieved from threshold to rollover lasing operation. The PhC VCSEL with trench demonstrated nearly 35 dB of SMSR. It is also noticed that the lasing wavelength is blue-shifted when trench and PhC air

Fig. 8. *L–I* characteristic for all fabricated VCSEL (typical, trench, and PhC with trench).

Fig. 9. *I–V* characteristic for all fabricated VCSEL (typical, trench, and PhC with trench).
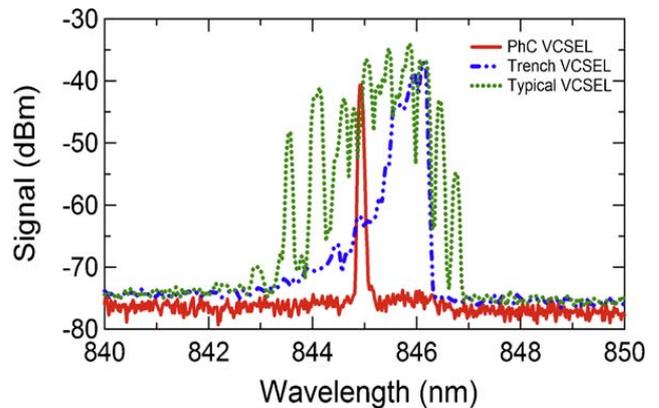

Fig. 10. Output spectrum for all fabricated VCSEL (typical, trench, and PhC with trench).
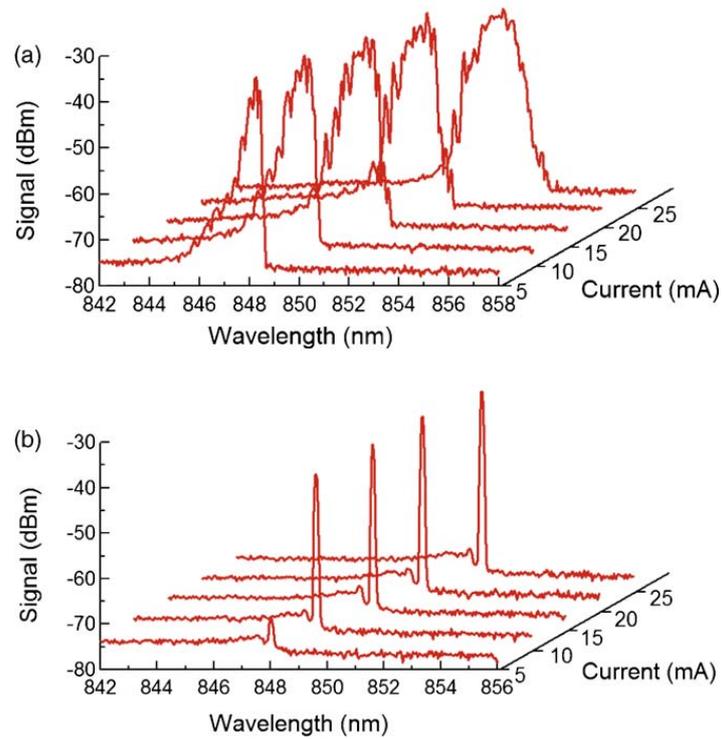
Fig. 11. Output spectrum for (a) typical VCSEL and (b) PhC VCSEL; at various injected currents.

holes are incorporated into the VCSEL. This effect could be contributed by the alteration of VCSEL cavity resonance due to the change of refractive index of the top DBR when trench and PhC air holes are introduced.

From the experiment measurement, only 50% of the total PhC VCSEL fabricated achieved single mode operation (SMSR > 35 dB) for devices with $a = 2.5$–4.5 μm ($b = 1.3$–2.3 μm). PhC VCSEL with smallest PhC air holes design ($a = 2.0$ μm and $b = 1.0$ μm) did not lase at all. This might be due to the incomplete fabrication of PhC air holes where etching difficulty exists for such small holes diameter. Other PhC VCSEL
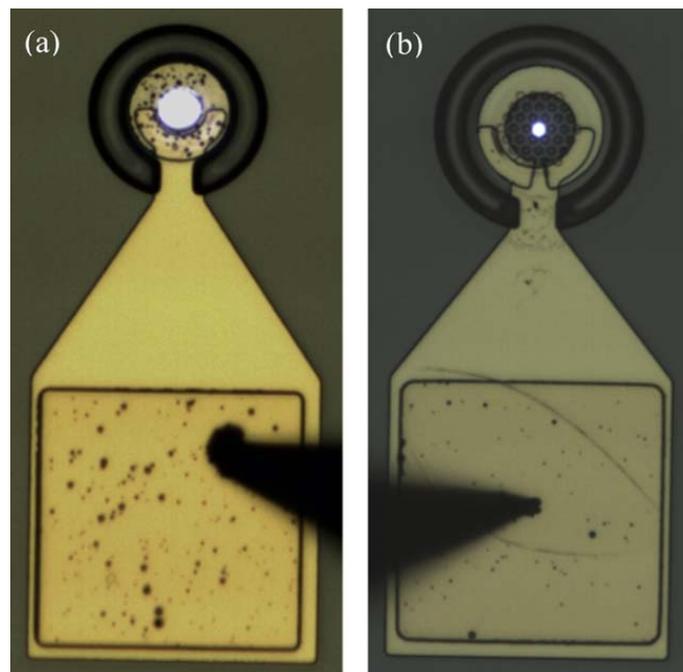

Fig. 12. Near-field comparison for (a) trench VCSEL and (b) PhC VCSEL with trench.

with larger PhC air holes designs ($a = 5.0$–6.5 μm and $b = 2.5$–3.3 μm) exhibits multimode spectrum. The large PhC air holes designs do not induce highly confined optical confinement (narrow step index profile), thus allowing the existence of high order modes in PhC VCSEL.

Fig. 11 demonstrates the output spectrum for both VCSEL samples T1 and T3 at various injected currents. PhC VCSEL with trench achieved single mode condition (SMSR > 30 dB) and narrow linewidth throughout the operating current range (above threshold current). No distinguish side modes appear at even high operating current. The typical oxide VCSEL shows multimode spectrum from low to high injection current levels. High number of transverse modes existed within the spectral wavelength range (840–852 nm). The spectrum also exhibits broadening linewidth as the injected current increased.

The near-field optical images comparison for both VCSEL samples T2 and T3 are shown in Fig. 12. The PhC VCSEL with trench structure demonstrates superior laser beam confinement at the centre of the PhC structure (no defect point) throughout the operating current range. Higher order modes are discriminated and only fundamental mode is allowed for lasing. As for the trench VCSEL without PhC structure, the laser beam is distributed across the entire VCSEL aperture. Due to this, the trench VCSEL exhibits higher output power compared to PhC VCSEL.

4. Conclusion

In this paper, we reported on significant approach to generate single transverse mode operation from a multimode GaAs-based oxide VCSEL by the means of PhC air holes and circular trench structure. The PhC design (in terms of lattice constant and holes diameter) is comprehensively studied using PWE and FDFD methods in order to induce single mode condition. The PhC design is then transferred to VCSEL device for experimental assessment. The fabricated PhC oxide VCSEL with etched trench successfully exhibits single mode output power of 0.7 mW, threshold current of 3.5 mA, slope efficiency of 0.10 W/A, and continuous single mode output spectrum at wide operating current range. Control oxide VCSEL devices in the form of typical air post mesa VCSEL and trench VCSEL (no PhC air holes) are also fabricated for comparison purpose. The PhC VCSEL with etched trench demonstrates an efficient combination approach to generate single transverse mode operation for VCSEL. This method is applicable to longer wavelength VCSEL (GaAs- or InP-based) since the PhC effect in obtaining single mode operation in VCSEL is independent to the laser operating wavelength [27].

References

[1] H. Soda, K. Iga, C. Kitahara, Y. Sumatsu, Jpn. J. Appl. Phys. 18 (1979) 2329.
[2] K. Iga, IEEE J. Quantum Electron. 6 (2000) 1201.
[3] F. Koyama, J. Lightwave Technol. 24 (2006) 4502.
[4] C.W. Wilmsen, H. Temkin, L.A. Coldren, Vertical-cavity Surface-emitting Lasers: Design, Fabrication, Characterization, and Applications, Cambridge Univ. Press, Cambridge, UK, 1999.
[5] P. Pepeljugoski, D. Kuchta, Y. Kwark, P. Pleunis, G. Kuyt, IEEE Photon. Technol. Lett. 14 (2002) 717.
[6] K.D. Choquette, K.L. Lear, R.P. Schneider, K.M. Geib, J.J. Figiel, R. Hull, IEEE Photon. Technol. Lett. 7 (1995) 1237.
[7] B. Weigl, M. Grabherr, C. Jung, R. Jager, G. Reiner, R. Michalzik, D. Sowada, K.J. Ebeling, IEEE J. Sel. Top. Quantum Electron. 3 (1997) 409.
[8] C. Jung, R. Jager, M. Grabherr, P. Schnitzer, R. Michalzik, B. Weigl, S. Muller, K.J. Ebeling, Electron. Lett. 33 (1997) 1790.
[9] R.A. Morgan, G.D. Guth, M.W. Focht, M.T. Asom, K. Kojima, L.E. Rogers, S.E. Callis, IEEE Photon. Technol. Lett. 4 (1993) 374.
[10] H. Martinsson, J.A. Vukusic, M. Grabherr, R. Michalzik, R. Jager, K.J. Ebeling, A. Larsson, IEEE Photon. Technol. Lett. 11 (1999) 1536.
[11] A. Haglund, J.S. Gustavsson, J. Vukusic, P. Modh, A. Larsson, IEEE Photon. Technol. Lett. 16 (2004) 368.
[12] E.W. Young, K.D. Choquette, S.L. Chuang, K.M. Geib, A.J. Fischer, A.A. Allerman, IEEE Photon. Technol. Lett. 13 (2001) 927.
[13] A. Furukawa, S. Sasaki, M. Hoshi, A. Matsuzono, K. Moritoh, T. Baba, Appl. Phys. Lett. 85 (2004) 5161.
[14] H.P.D. Yang, I.-C. Hsu, F.-I. Lai, H.C. Kuo, J.Y. Chi, Jpn. J. Appl. Phys. 45 (2006) L871.
[15] D.S. Song, S.H. Kim, H.G. Park, C.K. Kim, Y.H. Lee, Appl. Phys. Lett. 80 (2002) 3901.
[16] N. Yokouchi, A.J. Danner, K.D. Choquette, IEEE J. Sel. Top. Quantum Electron. 9 (2003) 1439.
[17] J.H. Baek, D.S. Song, I.K. Hwang, K.H. Lee, Y.H. Lee, Y. Ju, T. Kondo, T. Miyamoto, F. Koyama, Opt. Express 12 (2004) 859.
[18] A.J. Danner, J.J. Raftery Jr., P.O. Leisher, K.D. Choquette, Appl. Phys. Lett. 88 (2006) 091114.
[19] M.S. Alias, S. Shaari, P.K. Choudhury, S.M. Mitani, Laser Phys. 19 (2009) 1.
[20] T.A. Birks, J.C. Knight, P.S. Russell, Opt. Lett. 22 (1997) 961.

[21] A. Ferrando, E. Silvestre, J.J. Miret, P. Andres, M.V. Andres, Opt. Lett. 24 (1999) 276.

[22] Z. Zhu, T.G. Brown, Opt. Express 10 (2002) 853.

[23] G.P. Agrawal, Fiber-optic Communication Systems, Wiley, New York, USA, 1997.

[24] N. Yokouchi, A.J. Danner, K.D. Choquette, Appl. Phys. Lett. 82 (2003) 1344.

[25] D.F. Siriani, P.O. Leisher, K.D. Choquette, IEEE J. Quantum Electron. 45 (2009) 762.

[26] P.O. Leisher, A.J. Danner, K.D. Choquette, IEEE Photon. Technol. Lett. 18 (2006) 2156.

[27] A.M. Kasten, M.P. Tan, J.D. Sulkin, P.O. Leisher, K.D. Choquette, IEEE Photon. Technol. Lett. 20 (2008) 2010.